PHYSICAL REVIEW D VOLUME 44, NUMBER 11 1 DECEMBER 1991

Atmospheric electron flux at airplane altitude

R. Enomoto, J. Chiba, K. Ogawa, T. Sumiyoshi, and F. Takasaki
National Laboratory for High Energy Physics, KEK, 1-1 Oho, Tsukuba-city, Ibaraki 305, Japan

T. Kifune
Institute for Cosmic Ray Research, 3-2-1, Midori-cho, Tanashi-city, Tokyo 188, Japan

Y. Matsubara
Faculty of Science, Tokyo Institute of Technology, 2-12-1 Oookayama, Meguro-ku, Tokyo 152, Japan

J. Nishimura
Institute for Space and Astronautical Science, 3-1-1 Yunodai, Sagamihara-city, Kanagawa 229, Japan

(VEGA Collaboration)

(Received 16 April 1991)

We have developed a new detector to systematically measure the cosmic-ray electron flux at airplane altitudes. We loaded a lead-glass-based electron telescope onto a commercial cargo airplane. The first experiment was carried out using the air route between Narita (Japan) and Sydney (Australia); during this flight we measured the electron flux at various altitudes and latitudes. The thresholds of the electron energies were 1, 2, and 4 GeV. The results agree with a simple estimation using one-dimensional shower theory. A comparison with a Monte Carlo calculation was made.

I. INTRODUCTION

Atmospheric electrons are secondary products of atmospheric showers of γ rays from the decay of π^0's. These π's are also the secondary products of interactions of incident cosmic-ray nucleons with air. The parent π^0's are considered to decay at a few radiation lengths before the detection point of electrons. Thus, measurements of atmospheric electrons at airplane altitudes (200–300 mb) provide direct proof of the π production rate at the first interaction length in the air.

Measurements using an airplane have advantages. Systematic measurements at various altitudes and locations are possible. Thus, from the latitude dependence of the fluxes we can derive global information concerning the cutoff effect by the geomagnetic field; this information is seriously needed throughout the theoretical calculations [1]. Also, recent concern about radiation damage to the health of airplane crews means that a systematic measurement of cosmic-ray fluxes in the atmosphere at airplane altitudes is important.

Previous measurements had been carried out using emulsion chambers or ionization chambers [2]. In both cases, the statistics and systematics for GeV γ rays ($E < 10$ GeV) are not sufficient for the inputs of theoretical calculations. High-statistics data with known angles and positions are absolutely necessary.

If ambiguities in the theoretical calculations of cosmic rays in the atmosphere are reduced, applications can be expected, especially regarding ground-based γ-ray experiments.

II. CARGO AIRPLANE

The aircraft which we used was a B747F [3]. This plane is capable of flying at an altitude range from 9 to 13 km; further, the altitude can be arranged so as to accommodate the experimental requirements. There are three available spaces for freight: the upper, main, and lower decks. The main deck is suitable for larger, heavier instruments. In the main deck, the material located above is only an aluminum body, which is approximately 3 cm thick [$\sim 1/3$ radiation lengths (r.l.)] on the average (maximum rib thickness is 5 cm), which is negligibly small compared to an air thickness of 260 mb at 10 km. There are 33 lots in the main deck. We chose two in the center position where relatively heavy equipment can be loaded. The area is 243 cm$\times$680 cm and the height is 243 cm. The detector was loaded on a so-called 20-ft pallet, the size of which is 236 cm$\times$597 cm. The maximum weight was designed to be 11 tons. The pallet was firmly fixed to a rail parallel to the airplane axis; the detector was fastened to the pallet.

The aircraft has four 60-kV A power generators; approximately half of them are redundant for emergency purposes. After a precise power analysis, it became clear that we can easily use 4 kV A out of them. They are three-phased ac 110 V with a frequency of 400 Hz. The temperature and the pressure inside the main deck are the same as those of passenger aircraft. The temperature is well controlled at around $(23\pm1)°$ and the pressure is 0.7 atmosphere. We can therefore operate the detector as if it was a ground-based experiment.

Some of the most crucial parameters in this experiment are the direction, location, and altitude of the detector in real time. These are recorded within a so-called black box with high precision ($<0.5°$). The same data are transferred to a tape system called an aircraft integrated data system (AIDS) every one second [3]. The altitude is obtained by measuring the outside pressure; its precision is considered to be ± 15 m at 10 km. The other data are obtained by an inertial navigation system (INS) which has gyros within itself [3]. The angles of true heading, pitch, and roll are measured with an accuracy better than 0.5°. The latitude and longitude are calculated integrally from data concerning three-dimensional acceleration. The integrated error is approximated as $3+3T$ nautical miles (T in hour), which is negligibly small for our purpose. Also, each aircraft has a precision universal time (UT) clock; the time is also recorded by the AIDS. We can correctly derive this information by adjusting it to our clock after each experiment.

For an economical reason, we do not charter any aircraft, but use commercial freighter types. The detector is loaded as cargo, except for the fact that an ac power line is connected. The detector is designed to conform to various regulations.

III. DETECTOR

We have designed a lead-glass-based electron telescope (VEGA detector) [4,5]. We used DF6 [6] with a size of 120 mm×120 mm×300 mm. In total, 98 modules were combined and a surface area of 1680 mm×840 mm=1.41 m [2] obtained. The energy resolution, by itself, is $4\%/\sqrt{E}$ (E in GeV) and the stability is as good as 2% [7]. A cross-sectional view of the detector is shown in Fig. 1. The detector comprises hodoscopes at the top, followed by a Pb convertor, plastic scintillators (hadron hodoscopes), and lead-glass array at the bottom. The hodoscopes are made of two XY planes which are separated vertically by 1 m. The segmentation of each plane is 2 cm. The field of view is fully opened over a region as wide as $\pm 30°$ (in the direction of airplane axis). In the other direction, the detector sizes are limited by the aircraft space. Although the field of view is limited to $-15°$ to $+30°$, we can rotate the detector in either direction before flights. The field of view is calculated to be 2.03 sr geometrically and 0.935 sr by assuming a typical zenith-angle distribution of the cosmic rays at ~ 10 km.

Between the lead-glass array and hodoscopes, a Pb convertor of 1.5 r.l. ($=1/20$ interaction length) and plastic scintillators (hadron hodoscopes) are sandwiched in order to reduce the proton components in cosmic rays. Protons are efficiently rejected by looking at preshower development within the first radiation length. In order to check the rejection probability of hadrons and the electron efficiencies, we carried out a test experiment at the KEK Proton Synchrotron (PS) ($\pi 2$ beam line). The beam energies were 1.5, 2, and 3 GeV and four thicknesses (3, 6, 9, and 12 mm) of Pb convertors were tested. From the E/p of the lead-glass counter and the pulse height of the scintillator between the Pb convertor and the lead glass, we obtained the relationship between electron efficiencies versus hadron rejection factor as shown in Fig. 2. The final choice was a 9-mm-thick Pb convertor ($\sim 1.5X_L$). The hadron rejection probability was 98% while losing 7% of the electrons at 1.5-GeV energy. Although by this setup the energy resolution of the lead glass is deteriorated by this Pb convertor to approximately a 10% level, it does not affect the experimental principle.

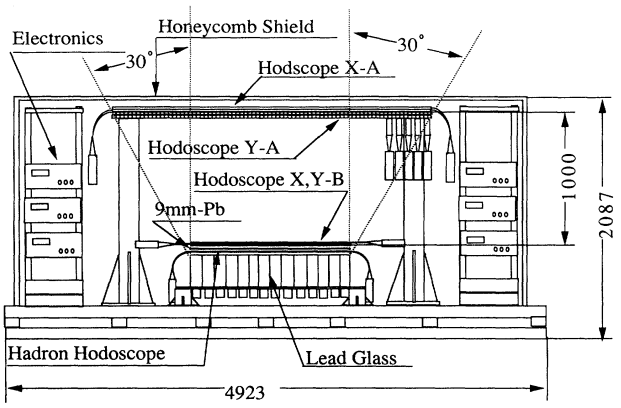

FIG. 1. Cross-sectional view of the VEGA detector.

We use standard electronics such as CAMAC, NIM, and VME, as is done in ground-based experiments. The hodoscopes are read by Lecroy ECLINE discriminators and latches. The other information, including that from the hadron hodoscopes and the lead-glass detectors, is fed to the CAMAC analog-to-digital converters (ADC's).

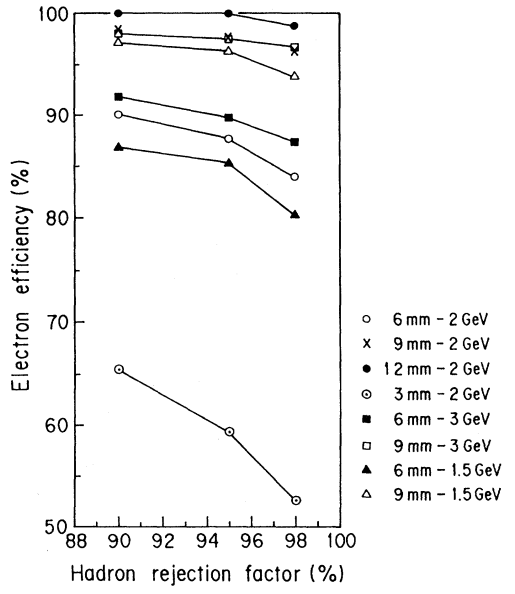

FIG. 2. The relationship between the hadron reflection probability and the electron efficiency. Three beam energies (1.5, 2, and 3 GeV) and four Pb thicknesses (3, 6, 9, and 12 mm) were tested.

Trigger logic is achieved by a combination of track signals from the hodoscopes and the pulse-height discrimination using the hadron hodoscopes and the lead-glass detectors. Online data taking is carried out by an NEC PC9801 personal computer; data are recorded on EXABYTE 8mm magnetic tape. The dead time is typically 20% for a trigger rate of 60 Hz. Each dc power supply is modified to fit ac 110 V, 400 Hz. The total power consumption is measured to be 4 kV A. We require no modifications of the aircraft's power system. In order to prevent any noise from the outside and to shut it out from the inside, all equipment is placed in a completely shielded case of aluminum honeycomb. This also serves to prevent the equipment from being disturbed in the case of some emergency, such as during a hard landing.

The whole structure must be able to tolerate acceleration in each direction to meet aircraft regulations. In the vertical and horizontal directions, which are perpendicular to the aircraft axis, the limits of maximum accelerations are 3 G. To the aircraft axis, i.e., the front and back, 9 G are the limits. We designed the detector system so as to fit such values. Especially, careful consideration is given to support of the lead-glass detectors. The total weight of the system becomes 7.8 tons for such reasons. The lead-glass detector themselves weigh only 2.5 tons.

IV. EXPERIMENT

The calibration of each counter was carried out using cosmic-ray muons triggered by coincidence of the hodoscopes on the ground. The trigger rate was ~150 Hz, consistent with previous measurements [8]. The energy deposited in a lead-glass detector by a vertical muon was about 200 MeV and the relative gain variation of each lead-glass counter was measured to be 2.3%. An absolute energy calibration was performed using an electron beam at the KEK accumulation ring (AR); the trigger threshold for the total energy deposit was set to 800 MeV. The relative gain of the hadron hodoscopes were also adjusted using cosmic-ray muons to be at a few-percent level.

In May 1989 we carried out an electromagnetic-interference test (EMI check) with a B747 at Narita International Airport with the cooperation of Japan Airlines Co. Ltd. (JAL).

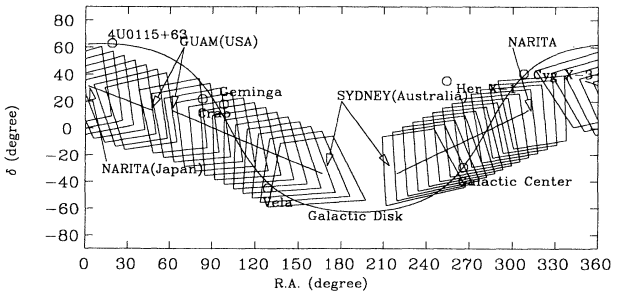

FIG. 3. Air route of JL 661 and 662. The lines are the movement of the zenith positions. The trapezoids show the full acceptance area of the VEGA detector every half an hour.

TABLE I. Experimental conditions.

Item	Value
Altitude range	9–13 km
Column density	220–300 g/cm^2
Longitude	~ const
Latitude	−30°–20°
Rigidity cutoff	4.5–16 GV
Energy threshold	1, 2, and 4 GeV

On 7 June 1989 (JST=Japan standard time = UT+9), the first flight was carried out between Narita (Japan) and Sydney (Australia) via Guam. The flight numbers were JL 661 and 662 which departed Narita at 6 a.m. The air route according to the equatorial coordinates is shown in Fig. 3. The experimental conditions are listed in Table I.

We tested three types of trigger modes.

Trigger 1. An electron mode which required a coincidence of the hodoscopes, the hadron hodoscopes ($>2\times$ minimum ionizing track) and the lead-glass counter (>800 MeV) from Narita to Guam.

Trigger 2. A charged-track mode by the hodoscope only from Guam to Narita.

Trigger 3. An electron-hadron mode which required the use of the hodoscopes and lead glass between Guam and Sydney.

The trigger rates are summarized in Table II along with the theoretical expectations, which can be found in Sec. V. The electron trigger rate changed rapidly at different altitudes, consistent with expectation. The proton contribution was roughly consistent with our expectation. The trigger rate of the charged tracks was obtained to be ~2 kHz at an altitude of 10 km above Narita. By correcting for the latitude effect we obtained a value roughly consistent with previous measurements [8]. For an atmospheric electron analysis, we used data obtained by trigger 3.

The electromagnetic cluster was reconstructed using the lead-glass array. The neighboring hits were combined within a cluster, where the energy threshold for each counter was 2.5 MeV (5× the noise level) and the hit position was calculated as a center of gravity. The position resolution was typically 40 mm. A minimum double-cluster separation was considered to be 37 cm. This kind of situation, however, was expected to rarely occur. The energy threshold for the lead-glass counter was set to various values (such as 940, 1930, and 3910 MeV) which

TABLE II. Trigger rates obtained by this experiment. Estimations described in the following section are also shown.

Altitude (km)	Pressure (mb)	Expt. Electron (Hz)	Theory Electron (Hz)	Expt. Proton (Hz)	Theory Proton (Hz)
10	265	45	48.1	17	12–26
11	227	60	61.0	24	16–33
12	194	75	72.8	29	20–33

correspond to incident electron energies of 1, 2, and 4 GeV at vertical incidence, respectively. The cluster in the hadron hodoscopes was reconstructed in the same way. The X position was obtained by the center of gravity and the Y position by the pulse-height ratio of two photomultipliers at both ends. The resolutions were 25 and 105 mm, respectively. The proton component was discriminated by the pulse height of the cluster. The threshold was set to 2.3 times the value of a minimum ionizing track. The final track fitting was performed by χ^2 minimization using the above-mentioned information. The χ^2 cut was set to 25, at which the degree of freedom was 4. The best χ^2 solution associated with a lead-glass cluster was selected as an electron candidate. The reconstruction efficiency was calculated to be 59.4% at 270 mb and 67.2% at 210 mb, respectively, by EGS4 simulations [9]. The altitude dependence originated from differences in the photon/electron ratios. Pair creation process at the airplane ceiling increases at a high photon/electron ratio (namely at high altitude) and these pairs were accepted as electron candidates. After these selections, 96.5% of the events had only a single track.

In order to check the angular resolution of this detector, we analyzed double-track events. Since the tracks were considered to come from the same shower, both must have had the same directions within the detector resolution. Figure 4 shows the angular difference of two tracks. In 1/3 of this sample, the tracks are parallel and the mean angular resolution $[(\sigma_x+\sigma_y)/2/\sqrt{2}]$ was obtained to be $0.98°\pm0.9°$, which is slightly worse than the estimated detector resolution ($\sim 0.5°$).

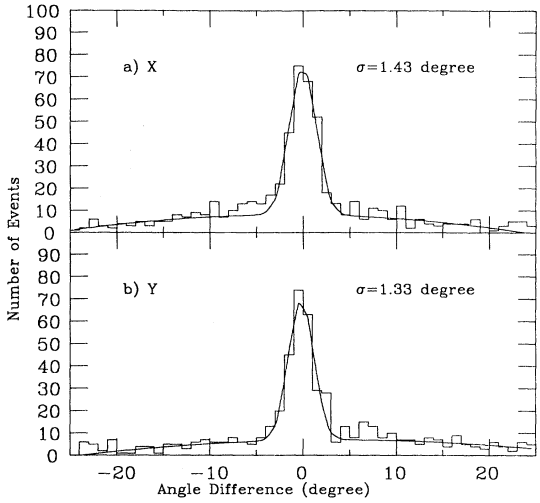

FIG. 4. The angular difference of two tracks in a sample of double-track events: (a) x direction and (b) y direction.

V. RESULTS

For an atmospheric electron analysis, we defined the cone to within 15° from the zenith. Since the pitch angle of airplane was as small as $+3°\pm1°$ and the roll angle was stable around $0°\pm0.5°$, the sensitivity inside the region defined above was always uniform. The electron flux was measured inside this region and is shown in Tables III, IV, and V. The integral flux is defined as

$$J=r(\theta<15°)/[d\Omega/(\text{area})/\text{time})]$$
$$=\int_{\theta<15°} j(\theta,\phi)\cos\theta\, d\Omega \Big/ \int_{\theta<15°}\cos\theta\, d\Omega$$
$$\sim j(0,\phi)\ ,$$

at various energy thresholds of 1, 2, and 4 GeV. Here, r

TABLE III. Integrated intensities (> 1 GeV) of atmospheric electrons at airplane altitude. The statistical error is typically 3% and the systematic error on the overall scale 5%.

$I(>1$ GeV) (10^{-4} cm^{-2}s^{-1}sr^{-1})	Latitude (deg)	Longitude (deg)	Rigidity cutoff (GV)	Column density (g/cm^2)
21.42±1.27	9.9	145.3	16.1	267.7
21.23±1.26	4.7	145.7	16.2	267.3
23.00±1.36	−0.4	146.2	16.1	267.4
22.09±1.31	−4.9	146.6	15.7	268.0
22.81±1.35	−10.2	147.5	14.9	268.2
22.27±1.32	−14.6	148.4	13.7	267.0
30.24±1.79	−19.3	149.5	10.8	221.6
29.81±1.76	−23.0	150.4	9.3	222.2
31.59±1.87	−26.7	150.9	7.3	222.0
33.75±2.00	−30.3	151.1	5.0	221.5
22.39±1.32	−28.2	151.2	6.2	293.5
21.80±1.29	−22.6	150.2	9.5	293.1
22.62±1.34	−17.0	148.8	12.3	267.5
23.03±1.36	−11.8	147.6	14.6	268.1
22.49±1.33	−6.5	146.7	15.5	258.7
23.04±1.36	−1.5	146.2	16.0	244.2
23.97±1.42	3.2	146.1	16.2	243.6
29.53±1.75	8.0	146.0	16.1	243.6

TABLE IV. Integrated intensities (> 2 GeV) of atmospheric electrons at airplane altitude. The statistical error is typically 3% and the systematic error on the overall scale 5%.

$I(>2$ GeV) (10^{-4} cm^{-2}s^{-1}sr^{-1})	Latitude (deg)	Longitude (deg)	Rigidity cutoff (GV)	Column density (g/cm^2)
8.44±0.50	6.3	145.7	16.2	267.6
9.21±0.54	0.7	146.2	16.2	267.4
8.06±0.48	−5.3	146.7	15.7	267.7
9.05±0.54	−11.2	147.8	14.7	267.8
9.11±0.54	−16.7	149.1	12.6	268.0
12.24±0.72	−22.6	150.4	9.5	221.8
11.58±0.69	−26.8	150.9	7.2	221.8
12.55±0.74	−30.8	151.2	4.8	221.8
8.28±0.49	−25.6	150.6	8.1	293.5
8.45±0.50	−19.1	149.2	10.9	279.2
8.89±0.53	−13.3	147.8	14.2	268.0
8.36±0.49	−7.2	146.7	15.4	266.0
9.79±0.58	−1.7	146.2	16.0	243.8
10.00±0.59	3.4	146.1	16.2	243.5
10.58±0.63	8.6	145.7	16.1	243.7

is the observed electron rate. The flux was obtained by accumulating 1000 events and by dividing the results by the time interval. Thus, the statistical error is typically 3%. The systematic uncertainty is considered to be less than 5%, which originated from the geometrical uncertainty, hadron contamination, and photon/electron ratio. Typically the proton incident events are 1/3 of the total events (trigger 3). After applying a hadron hodoscope cut, contamination of proton events is considered to be about 1.5%, which is negligibly small compared to the statistical error. The average altitude, latitude, and longitude during the measurement period are also shown in the tables. These values are consistent with the previous measurements [2].

In order to parametrize the γ-ray production rate, we approximate the latitude effect by

$$F_0/\gamma[1+b(\lambda-\lambda_0)^2E^{-\beta}]\ ,$$

and the altitude dependence by

$$\frac{1}{\Lambda}\sqrt{\gamma}M(\gamma)\left\{\frac{1}{1/\Lambda+\lambda_1}(e^{\lambda_1 T}-e^{-T/\Lambda})-\frac{1}{1/\Lambda+\lambda_2}(e^{\lambda_2 T}-e^{-T/\Lambda})\right\}\ ,$$

where λ and T are the latitude and air thickness in r.l., respectively. λ_0 is the latitude where the rigidity cutoff value becomes minimum within the air route (4.3N°). Λ is the attenuation length (a.l.), and a value of 100 g/cm^2~2.7 r.l. is used. The electron energy spectrum is parametrized as $E^{-\gamma}$. This formula is derived using the

TABLE V. Integrated intensities (> 4 GeV) of atmospheric electrons at airplane altitude. The statistical error is typically 3% and the systematic error on the overall scale 5%.

$I(>4$ GeV) (10^{-4} cm^{-2}s^{-1}sr^{-1})	Latitude (deg)	Longitude (deg)	Rigidity cutoff (GV)	Column density (g/cm^2)
2.93±0.17	8.2	145.7	16.1	269.1
2.98±0.18	2.7	146.2	16.2	267.6
2.93±0.17	−2.9	146.7	15.9	267.8
2.87±0.17	−8.7	147.7	15.2	267.9
3.15±0.19	−14.3	148.9	14.0	267.7
3.71±0.22	−19.4	150.0	10.9	235.8
4.08±0.24	−23.4	150.8	9.1	221.7
4.03±0.24	−27.4	151.1	6.8	221.5
2.60±0.15	−27.6	150.6	6.6	293.6
2.63±0.16	−21.0	149.1	9.9	287.4
2.98±0.18	−15.0	147.8	13.4	267.8
2.87±0.17	−9.2	146.7	15.1	267.5
3.33±0.20	−3.7	146.2	15.8	243.7
3.55±0.21	1.4	146.1	16.2	243.6
3.65±0.22	6.1	146.0	16.2	243.7

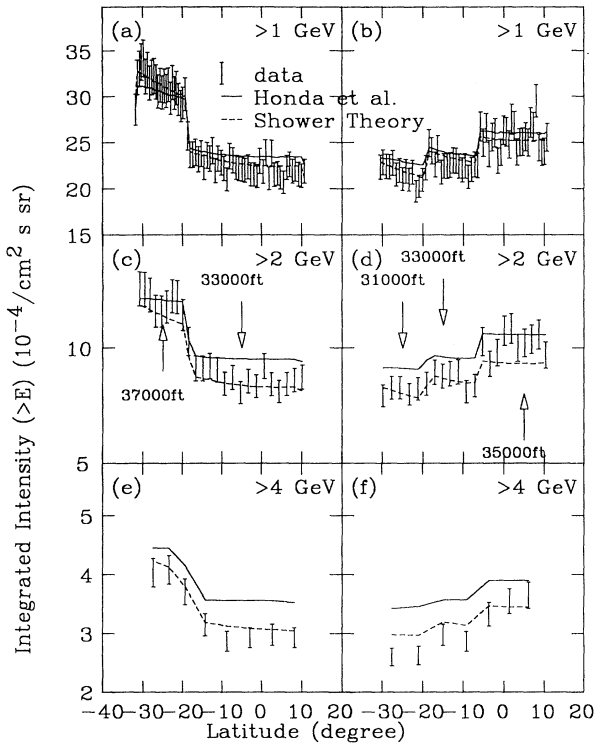

FIG. 5. Integrated intensity of atmospheric electrons. The horizontal axis represents the latitude. The energy thresholds are (a) and (b) 1 GeV (c) and (d) 2 GeV, and (e) and (f) 4 GeV, respectively. (a), (c), and (e) were obtained during flight from Guam to Sydney and (b), (d), and (f) during flight from the route from Sydney to Guam. The data with error bars represent the experimental; the solid curves were obtained by the Monte Carlo simulation by Honda *et al.* The dashed curves are the best-fit values according to the shower theory.

one-dimensional shower theory under the assumption that the altitude dependence of γ-ray production is $(1/\Lambda)e^{-t/\Lambda}$. The $M(\gamma)$, λ_1 and λ_2 are the shower functions described in the reference by Nishimura [10]. The variables are coefficients F_0, b, β, and γ. By fitting the data with this function, we obtained

$$F_0 = 3.43 \pm 0.02(\text{stat}) \pm 0.17(\text{syst}) \times 10^{-2}/\text{cm}^2\,\text{s sr GeV a.l.}\ ,$$

$$b = 1.43 \pm 0.11(\text{stat}) \times 10^{-4}/\text{deg}^2\ ,$$

$$\gamma = 1.4345 \pm 0.0015(\text{stat})\ ,$$

and

$$\beta = 0.17 \pm 0.21(\text{stat})\ .$$

The χ^2/N_{DF} was 111/167, respectively. The best-fit values are shown in Fig. 5 along with the experimental values.

The average zenith-angle distribution was obtained within the cone defined above. By fitting it with $\cos^n\theta$, we obtained the results shown in Table VI. The events which we accumulated correspond to come from the first interaction length on the average.

TABLE VI. The average angular distribution at the various latitudes and altitudes. The powers (n) of $\cos^n\theta$ are shown.

Altitude (ft)	Latitude range (deg)	n (expt.)	n (shower theory)
37 000	$9.9 \rightarrow -18.1$	0.41 ± 0.63	0.87
35 000	$-5.8 \rightarrow 10.7$	1.52 ± 0.60	1.09
33 000	$-19.3 \rightarrow -31.3$	1.15 ± 0.41	1.31
	$-18.5 \rightarrow -7.2$		
31 000	$-30.5 \rightarrow -20.1$	1.31 ± 0.67	1.56

VI. DISCUSSION

The atmospheric electrons are secondary products of the shower from the γ rays decayed from the π^0's. The π^0's are also secondary products of the interaction of cosmic-ray nucleons with air. Since the air density is sufficiently low compared to the hadron lifetime (when $E < 30$ GeV), the interactions of secondary unstable hadrons can be negligible. Thus, the π^0 production rate is considered to be proportional to the nucleon + air interaction rate $(1/\Lambda)e^{-T/\Lambda}$, where Λ is the attenuation length and is approximated to be 100 g/cm^2).

The atmospheric γ-ray flux has been measured by a balloon-borne experiment to be[11]

$$F(E) = 1.19 \times 10^{-4}(100\ \text{GeV}/E)^{2.72}/\text{m}^2\,\text{s GeV sr}$$

at 4 mb. At the balloon altitude ($\sim$ a few mb), the flux is considered to be proportional to $(1-e^{-t/\Lambda})$. Thus, the γ-ray production rate (>1 GeV) per unit attenuation length is considered to be

$$F_0 = 9.13 \times 10^{-2}/\text{cm}^2\,\text{s GeV sr a.l.}$$

at 1 GeV. Using our data, however, we obtained

$$F_0 = 3.81 \pm 0.02(\text{stat}) \pm 0.19(\text{syst}) \times 10^{-2}/\text{cm}^2\,\text{s sr GeV a.l.}$$

at a rigidity cutoff of 10 GV, which is smaller than that from the balloon-borne data. Using both data, the bending point of the energy spectrum was estimated to be 17.4–26.5 GeV. However, the measured spectrum was less steep ($\gamma \sim 1.43$) that $\gamma = 1.72$ and the energy threshold of the balloon-borne measurement was high (100 GeV). Also proton energy spectrum has a bend around this energy region. We consider that these effects reduced the electron fluxes at the 1-GeV threshold.

The zenith-angle distribution should be proportional to

$$J(T,\theta) = J(T/\cos\theta, 0) \propto (\cos\theta)^{(-T/J)(dJ/dT)}\ .$$

The value of $(-T/J)(dJ/dT)$ is calculated from shower theory and is shown in Table VI using the best-fit parameter of γ. The results are roughly consistent with the measurement.

The π^0 energies and the production points to which our γ-ray measurements correspond were estimated using the EGS4 simulation. The dominant contributions are

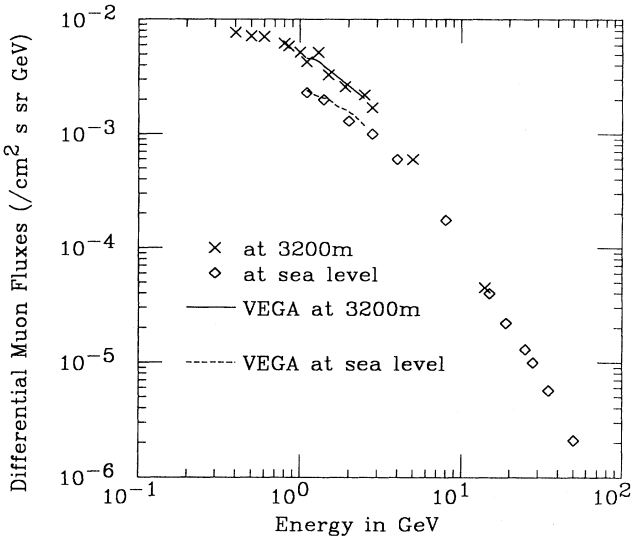

FIG. 6. Estimated fluxes of atmospheric muons at 3200 m (solid curve) and at sea level (dashed curve), together with the experimental data (symbols).

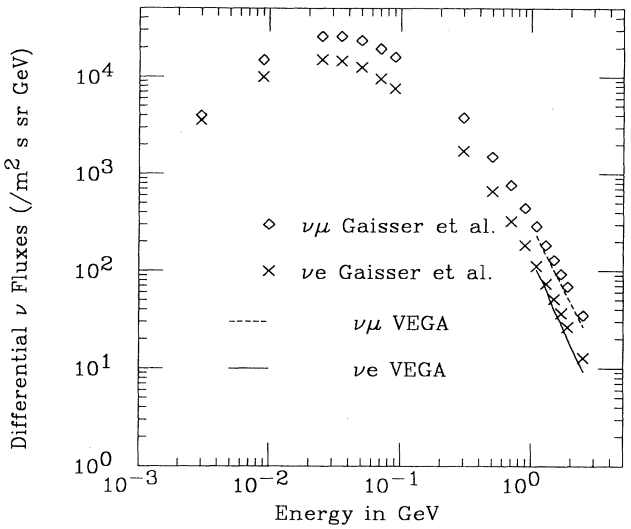

FIG. 7. Average neutrino fluxes $[(m^2 sr s)^{-1}]$. The data points were obtained by Gaisser *et al.* [1]. The upper are of ν_μ and the lower ν_e. The curves are the estimated results obtained from the VEGA experiment.

1–10 GeV π^0's and the mean production points were 130 mb. These regions are similar to that of atmospheric muon and neutrino production. Therefore we can roughly estimate the atmospheric muons and neutrinos of energy greater than 1 GeV. These fluxes are estimated using the following assumptions, based on a simple one-dimensional evaluation of $\pi \rightarrow \mu \rightarrow e$ cascade decays.

(1) The production probability of $\pi^{\pm}$ is twice of π^0.

(2) The differential energy spectrum of π^0 is proportional to $E^{-2.5}$ at $E > 1$ GeV.

(3) Phase-space decay is assumed in three-body decay.

(4) Intensities are calculated only using the vertical incidence of $\pi^{\pm}$, because the zenith-angle dependence is considered to be small [1].

(5) No secondary strong interaction of π is assumed.

(6) A uniform geomagnetic field of 0.3 G is assumed.

(7) The altitude dependence of the π production rate is proportional to $(1/\Lambda)e^{-t/\Lambda}$.

The atmospheric μ fluxes at 3200 m and at sea level were estimated and are shown in Fig. 6 along with the observed fluxes (solid line = 3200 m and dashed line = sea level [12], and are consistent with each other. Also, the atmospheric ν fluxes at underground were estimated, and are shown in Fig. 7 along with a calculation by Gaisser *et al.*[1] However, there are uncertainties in the primary cosmic-ray intensities especially due to solar modulations. Our measurement duration was limited to a day so that we cannot discuss this topic further.

We also compared the electron fluxes of our data and those of a Monte Carlo calculation by Honda *et al.* [13]. This would be a global check to the Monte Carlo method. Gaisser *et al.* compared their calculation with the experimental μ fluxes at various altitudes [1]. However, the energy determination and π discrimination were poor in the experimental results. On the other hand, regarding the electron fluxes, particle identification and energy determination are much better and the statistics are high. The results are shown in Fig. 5 by solid curves. The results agreed concerning the low-energy intensities, although there is a discrepancy of 7–30% in the 4-GeV data. The discrepancy was larger in the low altitude data (31 000 ft). Right now we do not have any conclusive arguments about this discrepancy. There are, however, possibilities of misunderstanding of the energy spectrum and/or attenuation length.

VII. CONCLUSION

We have developed a new detection method to measure the cosmic-ray electron flux in the atmosphere at airplane altitudes. We loaded a lead-glass-based electron telescope onto a commercial cargo airplane. The experiment was carried out using a flight between Narita (Japan) and Sydney (Australia) via Guam (U.S). The electron fluxes at various altitudes, latitudes, and thresholds were systematically measured. The statistical error of our measurement was typically 3%; the systematic error was estimated to be less than 5% at each measurement point. The measured electron fluxes are consistent with a simple estimation using one-dimensional shower theory. The γ-ray production probability per unit attenuation length and the energy spectrum around a few GeV were obtained. Also, regarding a systematic check of the above results, we compared our data with a calculation obtained by a sophisticated Monte Carlo simulation.

ACKNOWLEDGMENTS

We appreciate support from Professor H. Sugawara, Professor K. Kikuchi, Professor K. Takahashi, Professor

S. Iwata, Professor M. Kobayashi, Mr. Y. Ukita (KEK), Professor J. Arafune (ICRR), Dr. Y. Takahashi (Univ. of Alabama), Professor T. Kamae, and Dr. T. Takahashi (Univ. of Tokyo) in proceeding with this plan. We deeply thank Dr. M. Honda and Dr. K. Kasahara (ICRR) for their offer of Monte Carlo results. This work was partially supported by the Grant-in-Aid for Scientific Research on Priority Areas from the Japan Ministry of Education Science, and Culture. We thank Mr. T. Hakamada of Hamamatsu Photonics K. K. for cooperation. Finally we deeply appreciate Mr. M. Iizuka (Japan Airlines Co., Ltd.) for his substantial help and cooperation.

[1] T. K. Gaisser *et al.*, Phys. Rev. Lett. **51**, 223 (1983); T. K. Gaisser *et al.*, Phys. Rev. D **38**, 85 (1988).

[2] L. T. Baradzei *et al.*, J. Phys. Soc. Jpn. **17**, Suppl. A-III 433 (1961); J. Duthie *et al.*, Nuovo Cimento **24**, 122 (1962); L. T. Baradzei *et al.*, in *Proceedings of the International Conference on Cosmic Rays,* Jaipur, India, 1963, edited by R. R. Daniel *et al.* (Commercial Printing, Bombay, 1964-1965), Vol. 5, p. 283.

[3] M. Iizuka, Japan Airlines Co., Ltd. (private communication).

[4] R. Enomoto *et al.*, Nucl. Instrum. Methods **A295**, 261 (1990).

[5] R. Enomoto *et al.*, Phys. Rev. Lett. **64**, 2603 (1990).

[6] Nikon Catalogue, Nikon K. K., 3-2-3 Marunouchi, Chiyoda-ku, Tokyo, Japan.

[7] K. Ogawa *et al.*, Nucl. Instrum. Methods, **A243**, 58 (1986); T. Sumiyoshi *et al.*, *ibid.* **A271**, 432 (1988).

[8] S. Hayakawa, *Cosmic Ray Physics* (Wiley, New York 1969).

[9] W. R. Nelson *et al.*, SLAC Report No. 265, 1985 (unpublished).

[10] J. Nishimura, *Hand Book der Physik* (Springer, Berlin, 1987), Vol. 46, p. 1.

[11] J. Nishimura *et al.*, Astrophys. J. **238**, 394 (1980).

[12] J. Pine *et al.*, Nuovo Cimento **14**, 118 (1959); F. Ashton *et al.*, Nature **185**, 354 (1969); W. Pak *et al.*, Phys. Rev. **121**, 905 (1961); G. Brooke *et al.*, Proc. Phys. Soc. (London) **83**, 853 (1964).

[13] M. Honda *et al.*, Phys. Lett. B **248**, 1931 (1990).